

Observational constraints on a unified dark matter and dark energy model based on generalized Chaplygin gas

Chan-Gyung Park¹, Jai-chan Hwang¹, Jaehong Park¹, and Hyerim Noh²

¹*Department of Astronomy and Atmospheric Sciences, Kyungpook National University, Taegu, Korea*

²*Korea Astronomy and Space Science Institute, Daejeon, Korea*

(Dated: April 24, 2022)

We study a generalized version of Chaplygin gas as unified model of dark matter and dark energy. Using realistic theoretical models and the currently available observational data from the age of the universe, the expansion history based on the type Ia supernovae, the matter power spectrum, the cosmic microwave background radiation anisotropy power spectra, and the perturbation growth factor we put the unified model under observational test. As the model has only two free parameters in the *flat* Friedmann background [Λ CDM (cold dark matter) model has only one free parameter] we show that the model is already tightly constrained by currently available observations. The only parameter space extremely close to the Λ CDM model is allowed in this unified model.

PACS numbers: 98.80.-k, 95.36.+x

I. INTRODUCTION

A unified dark matter and dark energy model motivated by the (generalized) Chaplygin gas has been introduced in the literature [1, 2, 3], and has been extensively investigated in the cosmological studies [4, 5, 6, 7, 8, 9, 10, 11, 12, 13, 14, 15, 16, 17, 18, 19, 20, 21, 22, 23, 24, 25, 26, 27, 28, 29, 30, 31, 32, 33, 34, 35, 36, 37, 38, 39, 40]. Many constraints on the Chaplygin gas model parameters have been placed (predicted) based on current (upcoming) astronomical observations such as type Ia supernovae (SNIa) [4, 5, 6, 7, 8, 13, 14, 15, 17, 18, 19, 20, 23, 24, 25, 26, 27, 28, 29, 31, 33, 35], large-scale structure [6, 7, 8, 21, 22, 31, 37, 38, 40], cosmic microwave background radiation (CMB) [5, 7, 9, 10, 31, 36, 40], gravitational lensing [11, 14, 15, 20], gamma-ray bursts [30], X-ray luminosity of galaxy clusters [14, 19, 23], look-back time-redshift data [28, 39], angular size-redshift data [24], Hubble parameter-redshift data [34, 35], Fanaroff-Riley type IIb radio galaxies [14, 23], and so on.

It is known that such a unified model is constrained by observations so that parameter space close to the conventional Λ CDM models is allowed. But current status of the model in parameter space different from close-to- Λ CDM has been unclear. The distance-redshift relation, the age of the universe, abundances of light elements, the large-scale matter density and velocity power spectrum, the CMB temperature and polarization anisotropy power spectra, and the perturbation growth factor can be regarded as the main pillars of modern cosmology where theories meet with observations. Here, we investigate the unified model by comparing realistic theoretical predictions with currently available observations. Our conclusions can be found in section IV.

II. GENERALIZED CHAPLYGIN GAS

We introduce a fluid X with an equation of state

$$\tilde{p}_X = -A\tilde{\mu}_X^{-\alpha}, \quad (1)$$

where \tilde{p} and $\tilde{\mu}$ are the pressure and the energy density, and A and α are constants; tildes indicate covariant quantities. The Chaplygin gas is a case with $\alpha = 1$. It is interesting to note that any fluid with barotropic equation of state, $\tilde{p}_X = \tilde{p}_X(\tilde{\mu}_X)$, has an exact scalar field theory counterpart with a tachyonic kinetic term given by an action (we set $8\pi G \equiv 1 \equiv c$)

$$S = \int d^4x \sqrt{-\tilde{g}} \left[\frac{1}{2} \tilde{R} + \tilde{p}_X(\tilde{X}) \right], \quad \tilde{X} \propto e^{\int \frac{2d\tilde{p}_X}{\tilde{\mu}_X + \tilde{p}_X}}, \quad (2)$$

where $\tilde{X} \equiv \frac{1}{2} \tilde{\phi}^c \tilde{\phi}_{,c}$; see Appendix A for a proof. For a fluid in Eq. (1) we have

$$\tilde{p}_X \equiv -A^{\frac{1}{1+\alpha}} \left[1 - \left(\tilde{X}/B \right)^{\frac{1+\alpha}{2\alpha}} \right]^{\frac{\alpha}{1+\alpha}}, \quad (3)$$

where B is a constant. We call the fluid or field based on Eqs. (1) and (3), a generalized Chaplygin gas (GCG).

To the background order in Friedmann world model the energy conservation equation for GCG component gives

$$\begin{aligned} \mu_X &= \left(A + \frac{\mu_{X0}^{1+\alpha} - A}{a^{3(1+\alpha)}} \right)^{\frac{1}{1+\alpha}}, \quad p_X = -A\mu_X^{-\alpha} \\ w_X &\equiv \frac{p_X}{\mu_X} = - \left(1 + \frac{\mu_{X0}^{1+\alpha}/A - 1}{a^{3(1+\alpha)}} \right)^{-1}, \\ c_X^2 &\equiv \frac{\dot{p}_X}{\dot{\mu}_X} = -\alpha w_X, \end{aligned} \quad (4)$$

where a is the scale factor and $\mu_{X0}^{1+\alpha} > A$ (we set $a_0 \equiv 1$ at the present epoch). The equation of state

parameter w_X is negligible in the early era thus the GCG potentially acts as a dark matter, and approaches $w_{X0} = -A/\mu_{X0}^{1+\alpha} (> -1)$ in recent past thus it potentially acts as a dark energy depending on suitable choice of parameters.

We consider a *flat* background with baryon, radiation (photons and neutrinos), and the GCG. At the present epoch the Friedmann equation gives

$$\Omega_{X0} = 1 - \Omega_{b0} - \Omega_{r0}, \quad (5)$$

where $\Omega_i \equiv \mu_i/\mu_{crit}$ with μ_{crit} the critical density. Thus, μ_{X0} is completely fixed by the Friedmann equation. Equation (4) gives

$$A = -w_{X0}\mu_{X0}^{1+\alpha}. \quad (6)$$

As A is determined by w_{X0} and α , in the following we will regard w_{X0} and α as the two free parameters to be constrained by comparing the theoretical consequences with observations.

The Λ CDM limit can be reached by taking $\alpha = 0$, and identifying $A = \mu_\Lambda = \Lambda$ and $\mu_{c0} = \mu_{X0} - A$; μ_c indicates density of the CDM. Thus, in a flat background, from Eqs. (5) and (6) we have

$$w_{X0} = -\frac{\Omega_{\Lambda0}}{\Omega_{X0}} = -\frac{\Omega_{\Lambda0}}{\Omega_{\Lambda0} + \Omega_{c0}}. \quad (7)$$

We can show that even linear perturbation system (i.e., equations for δ_c and v_c) also coincides exactly with the Λ CDM case. As a fiducial model, we use flat Λ CDM model consistent with Wilkinson Microwave Anisotropy Probe (WMAP) 5-year data [41] ($\Omega_{b0} = 0.0456$, $\Omega_{c0} = 0.2284$, $\Omega_{\Lambda0} = 0.726$, $h = 0.705$, $n_s = 0.960$, $\sigma_8 = 0.812$, $T_0 = 2.725$ K, $Y_{He} = 0.24$, and $N_\nu = 3.04$), but without reionization history, see [42]. Thus we have $w_{X0} = -0.7607$.

In Fig. 1 we present the likelihood contours in α - w_{X0} plane based on the SNIa data. Also presented are the age lines. Notice that the likelihood contour as well as the age lines depend on Ω_{b0} in our GCG model. It is interesting to see that, except for small region close to the Λ CDM, most of the 1σ region based on SNIa can be ruled out by applying age of the universe larger than 13.5 Gyrs. Notice that the SNIa alone favors $\alpha = 0.9971$ and $w_{X0} = -0.8523$ (indicated by a bullet) which will be completely excluded by the matter and the CMB power spectra (see Fig. 3) and also by the age limit. Background evolutions for the locations indicated by \star in this Figure are presented in Fig. 2. Perturbation power spectra and the growth factors for the same parameters are presented in Figs. 3 and 4.

We consider scalar-type perturbations. For a fluid with barotropic equation of state we naturally have

$$\delta p_X = c_X^2 \delta \mu_X, \quad (8)$$

without the entropic perturbation. This relation is valid without taking any gauge condition. As the anisotropic

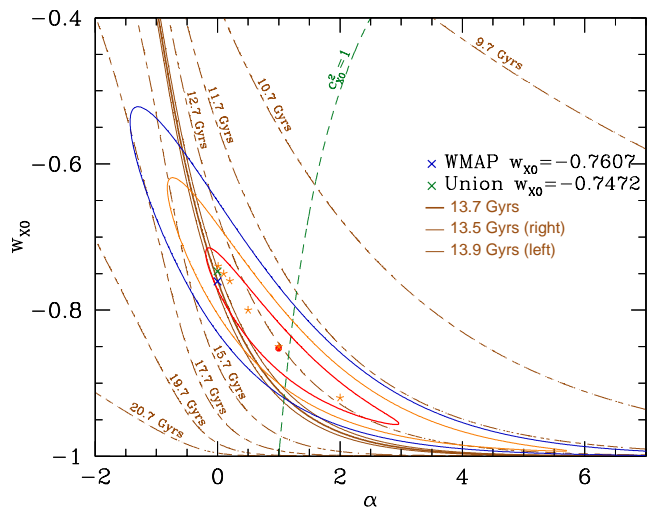


FIG. 1: Likelihood (1-3 σ) contours in α - w_{X0} plane based on the SNIa Union sample [43]. The locations of Λ CDM ($\alpha = 0$) based on the WMAP ($\Omega_{\Lambda0} = 0.726$) and Union data ($\Omega_{\Lambda0} = 0.713$) are indicated as \times . The maximum likelihood point is indicated by a bullet (\bullet). Locations indicated by \star are studied in details in Figs. 2-4. Locations near $\alpha = 0$ at $w_{X0} = -0.7607$ are studied in details in Figs. 5-7. We marginalized over the Hubble constant. Short-and-long-dashed lines are age lines in the unit of $(h/0.705)^{-1}$ Gyrs. The age lines together with the SNIa data already show that parameters with $\alpha > 0$ are largely excluded by currently available observations. A short-dashed line shows parameters which reach $c_{X0}^2 = 1$ at the present epoch; the right side of the line has $c_{X0}^2 > 1$ thus becoming super-luminal.

stress also vanishes the GCG is exactly an ideal fluid. Although the fluid definition of the GCG model is ambiguous about the ideal fluid nature, this can be proved by the field theoretic counterpart based on Eq. (2); see Appendix A for the proof. Without taking the temporal gauge condition the energy and the momentum conservation equations for the GCG become

$$\dot{\delta}_X = 3(w_X - c_X^2)H\delta_X + (1 + w_X)\left(\kappa - 3H\bar{\alpha} - \frac{k}{a}v_X\right), \quad (9)$$

$$\dot{v}_X = -(1 - 3c_X^2)Hv_X + \frac{k}{a}\frac{c_X^2}{1 + w_X}\delta_X + \frac{k}{a}\bar{\alpha}, \quad (10)$$

where $c_X^2 = -\alpha w_X$ for GCG; these are Eqs. (A7) and (A8) in [44] with $\delta_X \equiv \delta\mu_X/\mu_X$, v_X a perturbed velocity of GCG component, $\bar{\alpha}$ a perturbed metric variable and κ a perturbed part of the expansion scalar of the normal frame, see [47]; k is the comoving wave number.

III. OBSERVATIONAL CONSTRAINTS

In order to calculate the matter and CMB power spectra, and the baryon density perturbation growth factor

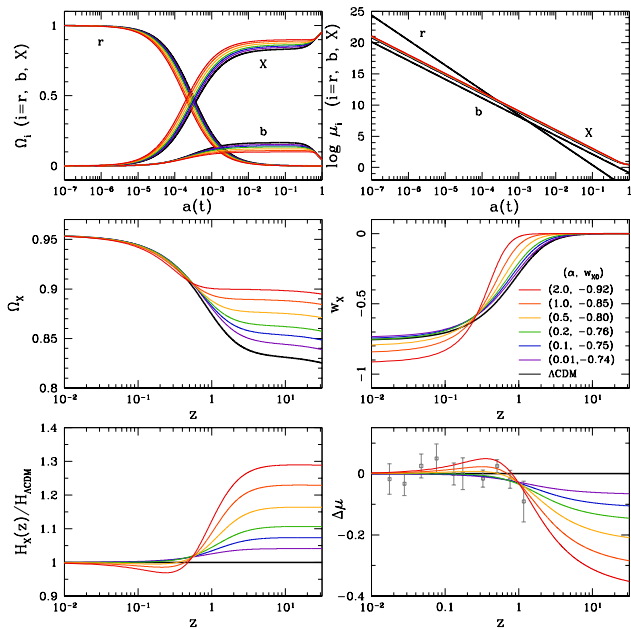


FIG. 2: Top panels: Evolution of Ω_i and μ_i as a function of scale factor $a(t)$ for values of (α, w_{X0}) indicated as \star in Fig. 1; $i = r, b, X$ indicates radiation, baryon, and GCG, respectively. Middle and bottom panels: Evolution of Ω_X , w_X , $H_X(z)/H_{\Lambda\text{CDM}}$ (H_X is the Hubble parameter in our GCG model), and the relative distance modulus $\Delta\mu(z) = \mu_X(z) - \mu_{\Lambda\text{CDM}}(z)$ for the same set of GCG parameters. In all panels, ΛCDM predictions are shown as thick black curves. In the $\Delta\mu$ -plot, the grey open squares with error bars represent the deviation of SNIa data points from the fiducial ΛCDM model considered here. The binned SNIa data are based on the Union sample [43].

we solve a system composed of baryon, radiation (handled using the Boltzmann equation or tight coupling approximation), together with the GCG described by Eqs. (9) and (10) representing the dark matter and the dark energy in a unified way. We consider a flat background with similar parameters as our fiducial ΛCDM model mentioned below Eq. (7) including neutrino components. Our set of equations and the numerical methods are presented in [45].

We solved the system in three different gauge conditions: the synchronous gauge (SG), the uniform-expansion gauge (UEG), and the uniform-curvature gauge (UCG); see [42, 47, 48] for the description of the gauges. The matter power spectrum and the perturbation growth factor are for the baryonic matter perturbation in the synchronous gauge which is a gauge-invariant concept in our situation. The CMB temperature and polarization anisotropies are naturally gauge invariant. The final results of these gauge-invariant variables calculated in our three different gauge conditions should coincide; this provides a numerical check of the calculations.

In Figs. 2 and 3 we present the background evolu-

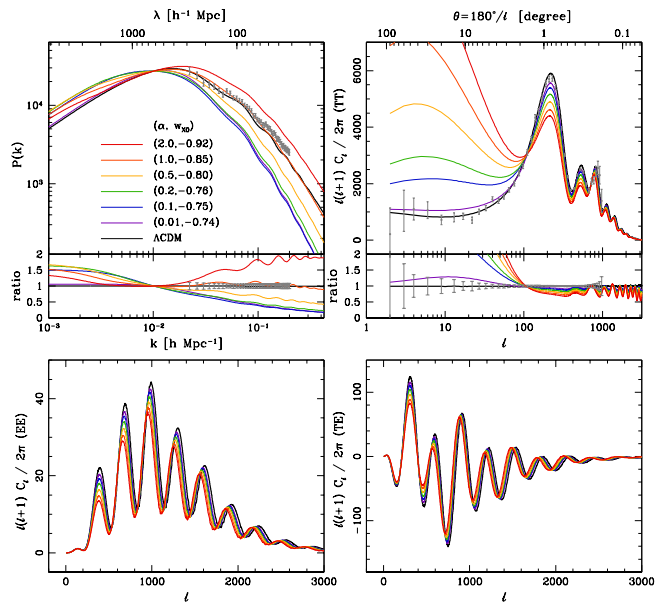


FIG. 3: The matter (baryon) power spectrum (top-left), and CMB TT (top-right), EE (bottom-left), TE (bottom-right) power spectra of GCG models with parameters used in Fig. 2, and the same colored code. All calculations are made in three different gauge conditions (SG, UEG, and UCG), and the results in the three gauges coincide exactly. The matter and CMB power spectra of the ΛCDM model have been normalized with σ_8 and COBE spectrum, respectively. For comparison, all the GCG power spectra have been normalized with the ΛCDM ones at $k = 0.01 h \text{ Mpc}^{-1}$ for matter power spectrum and $\ell = 700$ for CMB ones. The ratios of GCG powers to ΛCDM predictions are also shown in the bottom region of top panels. For matter and CMB TT power spectra, recent measurements from SDSS DR7 Luminous Red Galaxies (LRG) [46] and WMAP 5-year [41] data (including the cosmic variance) have been added (grey dots with error bars) together with fractional errors of observed spectra. For a correct comparison with the LRG band powers, the model power spectrum should include the convolution effect caused by LRG band power window functions and the non-linear clustering information.

tion, and the matter and the CMB power spectra for several typical parameters indicated as \star in Fig. 1. The bottom-right panel in Fig. 2 shows that all the parameters we consider fit well with the SNIa data. However, the power spectra in Fig. 3 show that all the GCG models we consider fail to fit the observed matter and CMB power spectra simultaneously. The baryon density perturbation growth factor presented in Fig. 4 also confirms this result.

Thus, we find that the only region in α - w_{X0} parameter space allowed by the current observations is the location close to ΛCDM . In order to constrain the observationally allowed variation of α in that region, in Figs. 5 and 6 we investigate the case of $-10^{-5} \leq \alpha \leq 10^{-2}$ for fixed $w_{X0} = -0.7607$. In Fig. 5 we present the matter and the

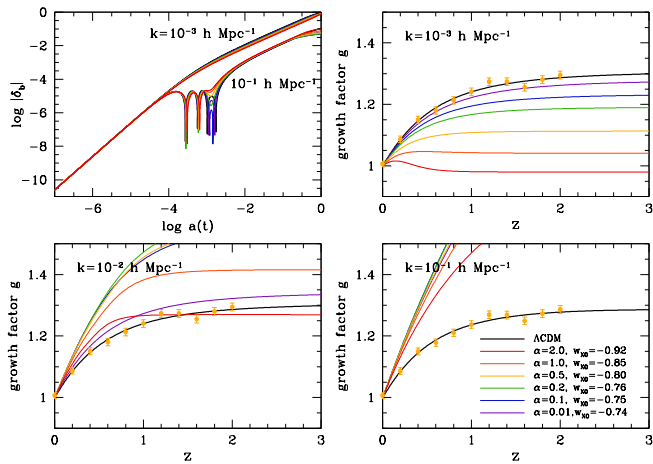


FIG. 4: Evolution of baryon density perturbation (top-left), and the normalized perturbation growth factor $g \equiv (\delta_b/a)$ in three different scales for the same parameters used in Figs. 2 and 3. We add 1% error bar expected from future X-ray and weak lensing observations [49].

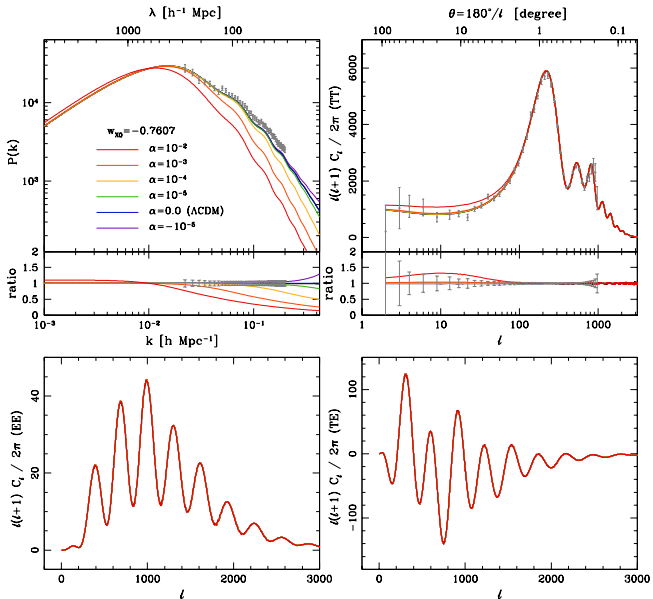


FIG. 5: The same as in Fig. 3 for values near $\alpha = 0$ (indicated in the Figure) with $w_{X0} = -0.7607$.

CMB power spectra; we do not present the background evolutions which are quite similar to the Λ CDM ones in Fig. 2. For the parameters considered the CMB power spectra are similar to the Λ CDM, thus observationally indistinguishable for $\alpha < 10^{-2}$. The matter power spectra in Fig. 5, however, depend more sensitively on the value of α . For example, for $\alpha > 10^{-4}$ the current observation can be used to distinguish its deviation. The baryon density perturbation growth factor presented in Fig. 6 also confirms this result which shows that the deviations are

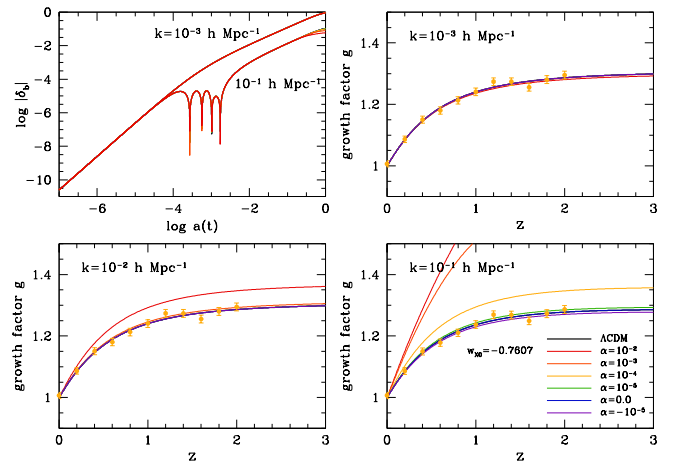


FIG. 6: The same as in Fig. 4 for the same parameters used in Fig. 5.

TABLE I: GCG model parameter constraints (68.3% CL) from SDSS DR7 LRG and Λ CDM-motivated mock power spectrum data based on likelihood distribution around $\alpha = 0$ (close to Λ CDM model).

	α	w_{X0}
LRG	$-5.98^{+11.3}_{-2.19} \times 10^{-5}$	$-0.756^{+0.023}_{-0.016}$
Λ CDM	$-0.25^{+5.78}_{-5.76} \times 10^{-6}$	$-0.7585^{+0.0035}_{-0.0030}$

particularly significant in the small scale.

Based on severe oscillations and divergent behaviors in the small scale of GCG power spectrum for nonvanishing α , authors of [22] concluded that $|\alpha|$ larger than 10^{-5} are excluded by the observation. This is understandable because the sound velocity squared c_X^2 becomes negative/positive, thus causing instability/oscillation for negative/positive α in the small-scale limit, see Appendix B for the analysis. However, later it has been shown that, despite the heavy oscillation and divergence of the GCG power spectrum, the accompanied baryon power spectrum behaves relatively well [8, 38]. In order to resolve the issue clearly, in Fig. 7 we present the baryon power spectra together with the GCG power spectra for the same parameters used in Fig. 5. The Figure confirms that despite the wild oscillations and divergences of GCG power spectra, the baryon power spectra behave much mildly. The Figure shows, however, that although $|\alpha| \sim 10^{-5}$ are surely acceptable, $\alpha \sim 10^{-4}$ gives deviation compared with current observation and $\alpha \sim 10^{-3}$ could be already excluded. For negative value of α we have more stringent limit so that $\alpha < -5.0 \times 10^{-5}$ already shows diverging behavior in the small scale limit.

In Figs. 5-7 we show that near $\alpha = 0$ (thus for GCG models close to Λ CDM) the observed matter power spectrum can be used to constrain tightly the allowed GCG models, whereas the CMB power spectra are relatively

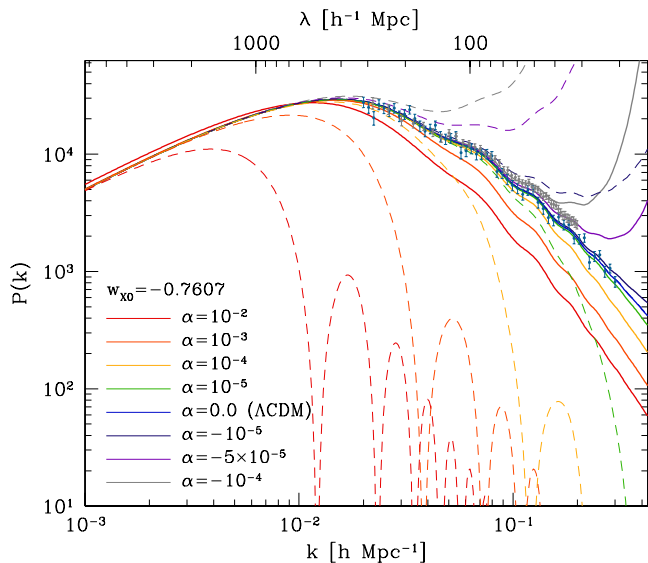


FIG. 7: The baryonic matter power spectrum in Fig. 5, together with the GCG power spectrum plotted in dashed lines. Although the baryon power spectra are normalized at $k = 0.01 h \text{ Mpc}^{-1}$, the GCG power spectra are normalized at $k = 0.001 h \text{ Mpc}^{-1}$ due to heavy oscillation of the latter ones. Compared with the GCG power spectra which oscillate significantly, baryon power spectra relatively behave mildly. The grey and blue dots with error bars represent the SDSS DR7 LRG and the ΛCDM mock power spectrum data, respectively. For the latter, we define 50 data points in the logarithmic interval between 0.02 and $0.3 h\text{Mpc}^{-1}$, and perturb the linear ΛCDM matter power spectrum at each point by adding a Gaussian noise with 10% of the power spectrum amplitude as standard deviation. This ΛCDM -motivated mock data will be used to constrain our GCG model in Fig. 8 and Table I.

similar to ΛCDM . In Fig. 8 we show the likelihood contours of GCG model parameters obtained from the SDSS DR7 LRG and ΛCDM -motivated mock power spectrum data in Fig. 7 (see Appendix C for the method). Table I lists 68.3% confidence limits (CL) of GCG model parameters estimated based on likelihood distribution around the narrow region close to ΛCDM model (inner panel of Fig. 8). Although not favored in the age constraint, we find another (besides the close-to- ΛCDM) region in the α - w_{X0} parameter plane where the matter power spectra are favored by current observations. In Fig. 9 we show the matter and the CMB power spectra for several parameters within 1σ domain in the matter power spectrum in Fig. 8. Authors of [38] showed that for large α with w_{X0} extremely close to -1 the matter power spectra are compatible with observation; this is consistent with our Fig. 8 (note that the truncation of contour at $\alpha \simeq 4.6$ is due to the finite bin size of w_{X0} used in the GCG model parameter search). However, our Fig. 9 shows that despite the observational success in the matter power spectra, significant deviations in the CMB power spectra are unavoidable, thus this additional domain is excluded by the

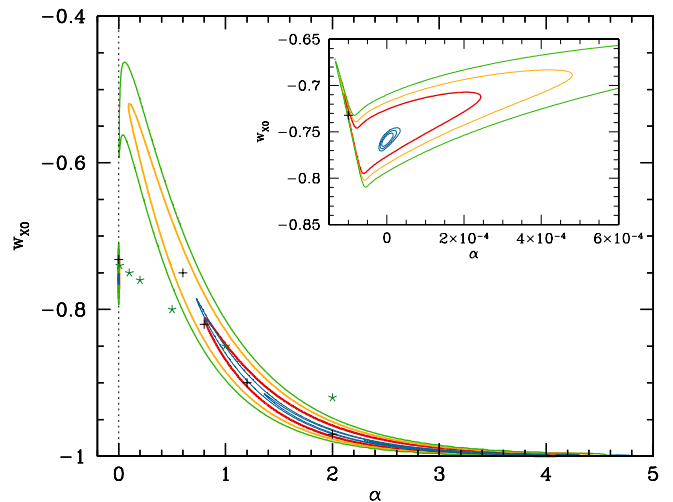


FIG. 8: Likelihood ($1-3\sigma$) contours in α - w_{X0} plane based on the matter power spectrum measurements from SDSS DR7 LRG [46] (red, yellow, green curves). For the method used, see Appendix C. Notice that besides the region around ΛCDM near $\alpha = 0$ (see the inner panel), the matter power spectrum favors another island with positive α . This island, however, can be excluded by the CMB power spectra in Fig. 9 and the age limit in Fig. 1. In the both panels, we add similar constraint based on ΛCDM -motivated mock power spectrum data in Fig. 7 (blue contours). GCG model parameters used in Figs. 2-4 are indicated by $*$; power spectra for several parameters consistent with LRG power spectrum indicated by $+$ are presented in Fig. 9.

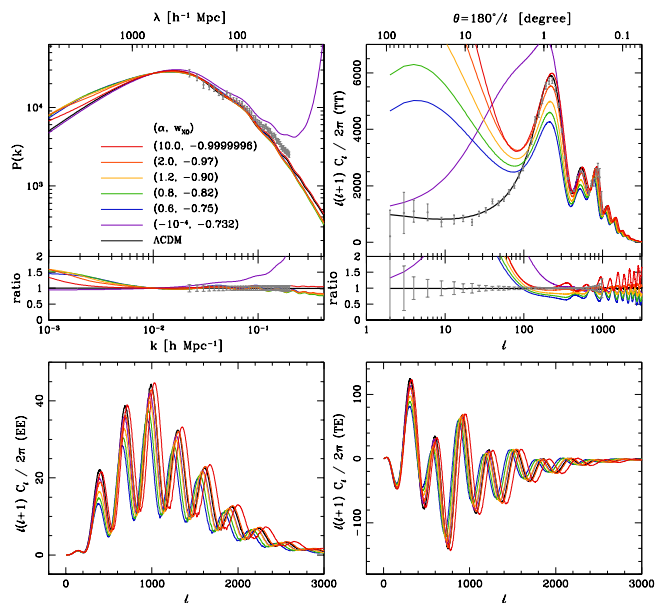


FIG. 9: The same as in Fig. 3 for parameters indicated. We present parameters which show similar behavior as the ΛCDM in the matter power spectra. All these models, however, show severe deviations in the CMB power spectra, thus are excluded.

CMB observations (in addition to the age test).

IV. DISCUSSION

We have systematically studied observational consequences of GCG unified dark matter and dark energy model. In the background Friedmann world model the basic requirement of minimum age of the universe together with the SNIa luminosity-redshift data already leaves only small parameter space close to the Λ CDM model, see Fig. 1. In the perturbation study, we have shown that the matter power spectrum and the CMB power spectra are mutually exclusive except for narrow region close to the Λ CDM model, see Figs. 3, 5, and 9. A tight constraint on α -parameter in that allowed region can be obtained from the (baryonic) matter power spectrum as $-5 \times 10^{-5} \leq \alpha \leq 10^{-4}$, see Figs. 5 and 7. More realistic constraint can be found in Fig. 8 and Table I as $|\alpha| \lesssim 10^{-4}$ from the SDSS DR7 LRG power spectrum and $|\alpha| \lesssim 10^{-5}$ from the Λ CDM mock power spectrum data. Although this allowed region is wider than what was concluded based on the GCG power spectrum in [22] (see Fig. 7), the constraint based on the baryon power spectrum is still severe enough so that the observationally allowed GCG model can be regarded as extremely close to the Λ CDM model, thus, effectively indistinguishable from the Λ CDM model. Although named as a unified model the GCG model has two free parameters, α and w_{X0} , whereas the Λ CDM has only one free parameter $\Omega_{\Lambda 0}$. From the perspective of more wider parameter space of our GCG model, it is remarkable to notice the distinguished success and its uniqueness of the Λ CDM model.

Acknowledgments

H.N. was supported by grants No. 2009-0078118 from Korea Science and Engineering Foundation (KOSEF). J.H. was supported by the Korea Research Foundation (KRF) Grant funded by the Korean Government (MOEHRD, Basic Research Promotion Fund) (No. KRF-2007-313-C00322) (KRF-2008-341-C00022), and by Grant No. R17-2008-001-01001-0 from KOSEF.

Appendices

Appendix A. Tachyonic field correspondence:

Action in Eq. (2) gives

$$\tilde{T}_{ab} = \tilde{p}_X \tilde{g}_{ab} - \tilde{p}_{X,X} \tilde{\phi}_{,a} \tilde{\phi}_{,b}. \quad (11)$$

Under the energy frame, with $\tilde{q}_a \equiv 0$, we have

$$\tilde{\mu} = -\tilde{p}_X + 2\tilde{p}_{X,X}\tilde{X}, \quad \tilde{p} = \tilde{p}_X, \quad \tilde{\pi}_{ab} = 0, \quad (12)$$

where the fluid quantities are defined in Eq. (2) of [50]. From $\tilde{\mu}_X = -\tilde{p}_X + 2\tilde{p}_{X,X}\tilde{X}$ we can derive

$$\tilde{X} \propto e^{\int \frac{2d\tilde{p}_X}{\tilde{\mu}_X + \tilde{p}_X}}. \quad (13)$$

Thus, for any barotropic fluid with $\tilde{p}_X = \tilde{p}_X(\tilde{\mu}_X)$ we have a corresponding tachyonic field with $\tilde{p}_X(\tilde{X})$ given by the above relation. To the background order, we have $c_X^2 \equiv \dot{p}_X/\dot{\mu}_X = p_{X,X}/\mu_{X,X}$. To the perturbed order, we have $\delta p_X = p_{X,X}\delta X$ and $\delta \mu_X = \mu_{X,X}\delta X$, thus $e_X \equiv \delta p_X - c_X^2 \delta \mu_X = 0$. As we have $e_X = 0$ and $\pi_{Xab} = 0$, the tachyonic field based on Eq. (2) corresponds to an ideal fluid.

Appendix B. Small-scale instability for $\alpha < 0$:

For $\alpha < 0$ we have $c_X^2 < 0$. As the GCG is an ideal fluid c_X can be interpreted as the sound velocity, and imaginary sound speed naturally leads to small scale instability. In order to show the instability we take the GCG-comoving gauge which sets $v_X \equiv 0$. Together with the Raychaudhury equation (see Eq. (A14) in [44])

$$\dot{\kappa} + 2H\kappa = -\left(3\dot{H} - \frac{k^2}{a^2}\right)\bar{\alpha} + 4\pi G(\delta\mu + 3\delta p), \quad (14)$$

Eqs. (9) and (10) lead to

$$\begin{aligned} & \ddot{\delta}_X + (2 - 6w_X + 3c_X^2)H\dot{\delta}_X \\ & - \left[3(5w_X - 3c_X^2)H^2 + 3(w_X + c_X^2)\dot{H}\right]\delta_X \\ & = \frac{1 + w_X}{a^2 H} \left[\frac{H^2}{a(\mu_X + p_X)} \left(\frac{a^3 \mu_X}{H} \delta_X \right) \right] \\ & + 4\pi G(1 + w)(1 + 3c_s^2)\mu\delta_X \\ & = 4\pi G(1 + w_X)(\delta\mu + 3\delta p) - c_X^2 \frac{k^2}{a^2} \delta_X, \end{aligned} \quad (15)$$

where $\delta\mu$ and δp are collective (total) perturbed energy density and perturbed pressure; $w \equiv p/\mu$ and $c_s^2 \equiv \dot{p}/\dot{\mu}$ where μ and p are collective (total) energy density and pressure of the background world model. We note that the above equation is generally valid in the presence of other components (baryon, radiation, etc.) and the background curvature. The presence of $c_X^2 k^2 \delta_X$ term in the right-hand-side of above equation shows that for negative/positive c_X^2 we have strong pressure-caused instability/oscillation in the small scale limit where k is large.

Appendix C. Likelihood estimation of GCG model parameters using the matter power spectrum data:

Here we briefly summarize how the likelihood contours of GCG model parameters in Fig. 8 have been obtained from the observed and mock power spectrum data. The power spectrum measured from SDSS DR7 LRG sample has been released recently [46], with 45 band power measurements at comoving scales $k = 0.0221\text{--}0.199 \text{ hMpc}^{-1}$, corresponding band-power window functions, and inverse covariance matrix between measurement errors. For each GCG model of α - w_{X0} , we obtain 45 data points by convolving the linear baryonic matter power spectrum with the band-power window functions and normalize the point at the largest

scale ($k = 0.0221 \text{ hMpc}^{-1}$) to that of (convolved) fiducial Λ CDM model power spectrum based on the WMAP 5-year observation. Then we estimate the GCG model probability distribution $\mathcal{L} \propto e^{-\chi^2/2}$ on α - w_{X0} plane by scanning $\chi^2 = \mathbf{d}^T \mathbf{C}^{-1} \mathbf{d}$, where \mathbf{d} is a 45×1 vector containing GCG powers relative to LRG measurement and \mathbf{C} is the 45×45 covariance matrix. During the scanning, other cosmological parameters have been fixed. By adding extremely large noise on the diagonal components of covariance matrix corresponding to $k > 0.1 \text{ hMpc}^{-1}$

scales, we have effectively excluded LRG power spectrum information at scales where non-linear clustering dominates. Notice that during the analysis we have completely ignored non-linear clustering properties of the matter power spectrum, and thus have not derived the halo power spectrum to compare with measured LRG power spectrum. For the case of Λ CDM-motivated mock power spectrum data (Fig. 8), similar analysis has been done but without convolution operations.

-
- [1] A.U. Kamenshchik, U. Moschella, and V. Pasquier, *Phys. Lett. B* **511**, 265 (2001).
- [2] N. Bilić, G.B. Tupper, and R.D. Viollier, *Phys. Lett. B* **535**, 17 (2002).
- [3] M.C. Bento, O. Bertolami, and A.A. Sen, *Phys. Rev. D* **66**, 043507 (2002).
- [4] U. Alam, V. Sahni, T.D. Saini, and A.A. Starobinsky, *Mon. Not. R. Astron. Soc.* **344**, 1057 (2003).
- [5] L. Amendola, F. Finelli, C. Burigana, and D. Carturan, *JCAP* **0307**, 005 (2003).
- [6] P.P. Avelino, L.M.G. Beça, J.P.M. de Carvalho, C.J.A.P. Martins, and P. Pinto, *Phys. Rev. D* **67**, 023511 (2003).
- [7] R. Bean and O. Doré, *Phys. Rev. D* **68**, 023515 (2003).
- [8] L.M.G. Beça, P.P. Avelino, J.P.M. de Carvalho, and C.J.A.P. Martins, *Phys. Rev. D* **67**, 101301 (2003).
- [9] M.C. Bento, O. Bertolami, and A.A. Sen, *Phys. Rev. D* **67**, 063003 (2003); M.C. Bento, O. Bertolami, and A.A. Sen, *Phys. Lett. B* **575**, 172 (2003); M.C. Bento, O. Bertolami, and A.A. Sen, *Gen. Rel. Grav.* **35**, 2063 (2003).
- [10] D. Carturan and F. Finelli, *Phys. Rev. D* **68**, 103501 (2003).
- [11] A. Dev, J.S. Alcaniz, and D. Jain, *Phys. Rev. D* **67**, 023515 (2003).
- [12] V. Gorini, A. Kamenshchik, and U. Moschella, *Phys. Rev. D* **67**, 063509 (2003).
- [13] M. Makler, S.Q. de Oliveira, and I. Waga, *Phys. Lett. B* **555**, 1 (2003).
- [14] M. Makler, S.Q. de Oliveira, and I. Waga, *Phys. Rev. D* **68**, 123521 (2003).
- [15] P.T. Silva, and O. Bertolami, *Astrophys. J.* **599**, 829 (2003).
- [16] M.C. Bento, O. Bertolami, and A.A. Sen, *Phys. Rev. D* **70**, 083519 (2004).
- [17] O. Bertolami, A.A. Sen, S. Sen, and P.T. Silva, *Mon. Not. R. Astron. Soc.* **353**, 329 (2004).
- [18] R. Colistete, J.C. Fabris, S.V.B. Gonçalves, and P.E. de Souza, *Int. J. Mod. Phys. D* **13** 669 (2004).
- [19] J.V. Cunha, J.S. Alcaniz, and J.A.S. Lima, *Phys. Rev. D* , **69**, 083501 (2004).
- [20] A. Dev, D. Jain, and J.S. Alcaniz, *Astron. Astrophys.* **417** 847 (2004).
- [21] T. Multamäki, M. Manera, and E. Gaztañaga, *Phys. Rev. D* **69**, 023004 (2004).
- [22] H. Sandvik, M. Tegmark, M. Zaldarriaga, and I. Waga, *Phys. Rev. D* **69**, 123524 (2004).
- [23] Z.-H. Zhu, *Astron. Astrophys.* **423**, 421 (2004).
- [24] J.S. Alcaniz, and J.A.S. Lima, *Astrophys. J.* , **618**, 16 (2005).
- [25] M.C. Bento, O. Bertolami, N.M.C. Santos, and A.A. Sen, *Phys. Rev. D* **71**, 063501 (2005).
- [26] M. Biesiada, W. Godłowski, and M. Szydlowski, *Astrophys. J.* **622**, 28 (2005).
- [27] R. Colistete, and J.C. Fabris, *Class. Quant. Grav.* **22**, 2813 (2005).
- [28] Y. Gong, *JCAP* **0503**, 007 (2005).
- [29] R. Lazkoz, S. Nesseris, and L. Perivolaropoulos, *JCAP* **0511**, 010 (2005).
- [30] O. Bertolami, and P.T. Silva, *Mon. Not. R. Astron. Soc.* **365**, 1149 (2006).
- [31] X. Zhang, F.-Q. Wu, and J. Zhang, *JCAP* **0601**, 003 (2006).
- [32] H. Zhang, and Z.-H. Zhu, *Phys. Rev. D* **73**, 043518 (2006).
- [33] Z.-K. Guo, and Y.-Z. Zhang, *Phys. Lett. B* **645**, 326 (2007).
- [34] P. Wu, and H. Yu, *Phys. Lett. B* **644**, 16 (2007).
- [35] P. Wu, and H. Yu, *JCAP* **0703**, 015 (2007).
- [36] T. Barreiro, O. Bertolami, and P. Torres, *Phys. Rev. D* **78**, 043530 (2008).
- [37] J.C. Fabris, S.V.B. Gonçalves, H.E.S. Velten, and W. Zimdahl, *Phys. Rev. D* , **78**, 103523 (2008).
- [38] V. Gorini, A.Y. Kamenshchik, U. Moschella, O.F. Piattella, and A.A. Starobinsky, *JCAP* **0802**, 016 (2008).
- [39] Z. Li, P. Wu, and H. Yu, *JCAP* **0909**, 017 (2009).
- [40] Y. Urakawa, and T. Kobayashi, arXiv:0907.1191 (2009).
- [41] G. Hinshaw *et al.*, *Astrophys. J. Suppl.* **180**, 225 (2009); M.R. Nolta, *et al.*, **180**, 296 (2009).
- [42] C.-G. Park, J. Hwang, J. Lee, and H. Noh, *Phys. Rev. Lett.* In press (2009).
- [43] M. Kowalski *et al.*, *Astrophys. J.* **686**, 749 (2008).
- [44] J. Hwang and H. Noh, *Phys. Rev. D* **64**, 103509 (2001).
- [45] J. Hwang and H. Noh, *Phys. Rev. D* **65**, 023512 (2002).
- [46] B.A. Reid *et al.*, arXiv:0907.1659v2 (2009).
- [47] J.M. Bardeen, *Particle Physics and Cosmology*, edited by L. Fang, and A. Zee, (Gordon and Breach, London, 1988), p1; J. Hwang, *Astrophys. J.* **375**, 443 (1991).
- [48] J.M. Bardeen, *Phys. Rev. D* **22**, 1882 (1980).
- [49] A. Vikhlinin *et al.*, astro-ph/0903.5320 (2009).
- [50] J. Hwang, *Class. Quant. Grav.* **7**, 1613 (1990).